Ticks and Tick-borne Diseases 15 (2024) 102287

Contents lists available at ScienceDirect

Ticks and Tick-borne Diseases

journal homepage: www.elsevier.com/locate/ttbdis

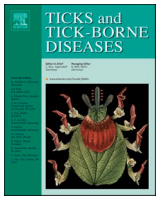

Original article

Structural studies of chromosomally encoded outer surface lipoprotein BB0158 from *Borrelia burgdorferi* sensu stricto

Kalvis Brangulis *, Inara Akopjana, Janis Bogans, Andris Kazaks, Kaspars Tars

Latvian Biomedical Research and Study Centre, Ratsupites 1 k-1, Riga LV-1067, Latvia

ARTICLE INFO

Keywords:
Lyme borreliosis
Spirochetes
X-ray crystallography

ABSTRACT

Lyme disease, or also known as Lyme borreliosis, is caused by the spirochetes belonging to the *Borrelia burgdorferi* sensu lato complex, which can enter the human body following the bite of an infected tick. Many membrane lipid-bound proteins, also known as lipoproteins, are located on the surface of *B. burgdorferi* sensu lato and play a crucial role in the spirochete to interact with its environment, whether in ticks or mammals. Since the spirochete needs to perform various tasks, such as resisting the host's immune system or spreading throughout the organism, it is not surprising that numerous surface proteins have been found to be essential for *B. burgdorferi* sensu lato complex bacteria in causing Lyme disease. In this study, we have determined (at 2.4 Å resolution) and characterized the 3D structure of BB0158, one of the few chromosomally encoded outer surface proteins from *B. burgdorferi* sensu stricto. BB0158 belongs to the paralogous gene family 44 (PFam44), consisting of four other members (BB0159, BBA04, BBE09 and BBK52). The characterization of BB0158, which appears to form a domain-swapped dimer, in conjunction with the characterization of the corresponding PFam44 members, certainly contribute to our understanding of *B. burgdorferi* sensu stricto proteins.

1. Introduction

Borrelia burgdorferi sensu lato complex bacteria (includes *Borrelia burgdorferi* sensu stricto (hereafter *B. burgdorferi*), *Borrelia afzelii, Borrelia garinii, Borrelia spielmanii, Borrelia bavariensis* and *Borrelia mayonii*) are the causative agents of Lyme borreliosis, which can be transmitted to mammalian organisms through the bite of infected *Ixodes* species ticks during their feeding (Baranton et al., 1992; Burgdorfer et al., 1982; Hu et al., 2001; Margos et al., 2013; Pritt et al., 2016; Radolf et al., 2012; Rudenko et al., 2011; Stanek and Reiter, 2011). *Borrelia burgdorferi* is a spirochete with an unusual genome. For instance, the genome of the *B. burgdorferi* strain B31 consists of a linear chromosome of approximately 900 kbp and 12 linear and 9 circular plasmids of around 600 kbp (Casjens et al., 2012). However, it has been demonstrated that clinical isolates from Lyme disease patients and in vitro cultivation can result in the loss of plasmids, leading to considerable variation in the plasmid composition of the spirochete (Casjens et al., 2017; Iyer et al., 2003). *Borrelia burgdorferi* has a complex life cycle in which certain *Ixodes* species ticks play an important role. The life cycle of *Ixodes* species ticks consists of four life stages: egg, larva, nymph, and adult. During the larval stage, these ticks feed on diverse land vertebrates, potentially becoming infected with *B. burgdorferi* if the host animal carries the bacteria. In the following year, ticks progress to the nymphal stage and can transmit *B. burgdorferi* to the host during feeding. As nymphs mature into adults, they require a final blood meal to facilitate egg-laying (Anderson, 1989). Meanwhile, *B. burgdorferi* must adapt to different environments, whether within a tick or a mammalian organism. Therefore, in order to perform various tasks, including resisting the host's immune system or attaching to host surfaces, it is not surprising that *B. burgdorferi* has around 130 proteins covalently attached to the fatty acids in the membrane bilayer via Cysteine (Cys) residue after the cleavage of the N-terminal signal peptide (Setubal et al., 2006; Zückert, 2014). These proteins, known as lipoproteins, can be located in both the periplasm and on the outer surface. Among these lipoproteins, approximately 90 are exposed on the outer surface, but only 7 of them (BB0158, BB0171, BB0213, BB0352, BB0689, BB0758, and BB0823) are encoded on the linear chromosome (Dowdell et al., 2017). While the exact function of these 7 surface-exposed lipoproteins remains undetermined, structural characterization has been performed on BB0689 (Brangulis et al., 2015). In the current study, we have solved the crystal structure of BB0158 to gain molecular insights into the chromosomally encoded, surface-localized protein that potentially plays a role in the pathogenesis

* Corresponding author.
E-mail address: kalvis@biomed.lu.lv (K. Brangulis).

https://doi.org/10.1016/j.ttbdis.2023.102287
Received 24 September 2023; Received in revised form 21 November 2023; Accepted 22 November 2023
Available online 27 November 2023

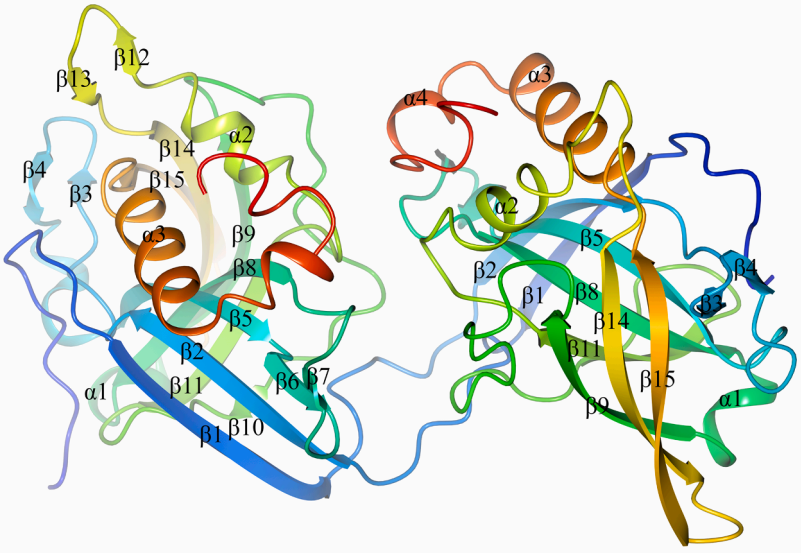

Fig. 1. The overall structure of *B. burgdorferi* BB0158 (PDB ID 8Q4K). BB0158 domain-swapped homodimer as observed in the crystal structure. The structure for each protomer is colored from blue at the N-terminus to red at the C-terminus. The four α-helices are marked from α1 to α4 and the fifteen β-strands are marked from β1 to β15.

of Lyme disease. Additionally, BB0158 is a member of the paralogous gene family 44 (PFam44), one of approximately 150 paralogous gene families found in *B. burgdorferi* B31 (Casjens et al., 2000). The characterization of BB0158, which appears to form a domain-swapped dimer, along with insights into PFam44, undoubtedly contributes to our understanding of *B. burgdorferi* proteins. Given that surface proteins may play an essential role in the pathogenesis of Lyme disease and can be valuable in vaccine development, further research on this protein is expected to be conducted.

2. Materials and methods

2.1. Cloning, expression and purification of BB0158

The gene encoding protein BB0158$_{29–238}$ (UniProtKB: O51180) was amplified by PCR from genomic DNA of *B. burgdorferi* B31, excluding both the signal sequence coding region and part of the predicted flexible N-terminal segment. The product was ligated into the pETm-11 expression vector resulting in a construct coding for an N-terminal 6xHis tag followed by a tobacco etch virus (TEV) protease cleavage site. BB0158$_{29–238}$ was expressed in *Escherichia coli* BL21 (DE3) as described previously for *B. burgdorferi* protein BBA14 (Akopjana and Brangulis, 2022). Protein purification and 6xHis tag removal was carried out as described previously for *B. burgdorferi* BBA65 and *B. spielmanii* A14S BSA64 (ORF name: *BSPA14S_A0059*) (Brangulis et al., 2020). Briefly, the supernatant obtained after the centrifugation of cell lysate at 10 000 rpm for 30 min was loaded on a Ni-NTA agarose (Qiagen, Hilden, Germany) gravity-flow column. The column was washed with 25 mM imidazole (pH 7.0), 300 mM NaCl and 20 mM NaH_2PO_4 and the recombinant BB0158 was eluted in 300 mM imidazole (pH 7.0), 300 mM NaCl and 20 mM NaH_2PO_4. The resulting protein fraction was buffer-exchanged into 10 mM Tris–HCl (pH 8.0) using an Amicon centrifugal filter unit (Millipore, Burlington, MA, USA). To remove the 6xHis tag, the buffer-exchanged protein fraction was mixed with recombinant tobacco etch virus (TEV) protease and incubated overnight at room temperature prior to transfer onto a Ni-NTA agarose (Qiagen, Hilden, Germany) column to remove the TEV protease and the cleaved 6xHis tag. Ultimately BB0158$_{29–238}$ was at a concentration of 8 mg/ml in 10 mM Tris–HCl (pH 8.0) buffer.

2.2. Crystallization of BB0158

Crystallization trials of BB0158 were performed in 96-well sitting drop plates (SWISSCI AG, Neuheim, Switzerland) by using the 96-reagent sparse-matrix screens JCSG+ and Structure Screen 1&2 (Molecular Dimensions, Newmarket, UK). Sitting drops were prepared by mixing 0.4 µl of protein (8 mg/ml) with 0.4 µl of precipitant using a Tecan Freedom EVO100 workstation (Tecan Group, Männedorf, Switzerland). Initial crystal hits were manually optimized and the best diffracting crystals were grown using the precipitant solution containing 0.2 M ammonium sulfate, 0.1 M sodium acetate (pH 4.6) and 20 % PEG 2000 MME. Addition of 15 % glycerol was used a cryoprotectant before transferring the crystals to liquid nitrogen and data collection.

2.3. Data collection and structure determination

Diffraction data were collected at the MX beamline instrument BL 14.1 at Helmholtz-Zentrum, Berlin (Mueller et al., 2012). Reflections were indexed by XDS and scaled by AIMLESS from the CCP4 suite (Evans, 2011; Kabsch, 2010; Winn et al., 2011). Molecular replacement using Phaser software (McCoy et al., 2007) was used to obtain phase information. AlphaFold (Jumper et al., 2021) generated protein prediction model was used as a search model. The protein structure was improved automatically in BUCCANEER followed by manual rebuilding in COOT (Cowtan, 2006; Emsley and Cowtan, 2004). Crystallographic refinement was performed using REFMAC5 (Murshudov et al., 1997). A summary of the data collection, refinement and validation statistics for BB0158 is given in **Table S1.**

2.4. Protein 3D structure prediction using AlphaFold

AlphaFold v2.0 (Jumper et al., 2021) was used to predict the 3D structures and the respective oligomers for BB0158 (UniProtKB: O51180), BB0159 (UniProtKB: O51181), BBA04 (UniProtKB: O50898), BBE09 (UniProtKB: O50705) and BBK52 (UniProtKB: O50852). Structure prediction with AlphaFold v2.0 was performed according to the default parameters as indicated at the website https://github.com/deepmind/alphafold/ running on AMD Ryzen Threadripper 2990WX 32-Core; 128 GB RAM; 4 x NVIDIA GeForce RTX 2080, and using the full databases downloaded on 2022–09–25. For further structural analysis, only the predicted structure with the highest confidence was used (as

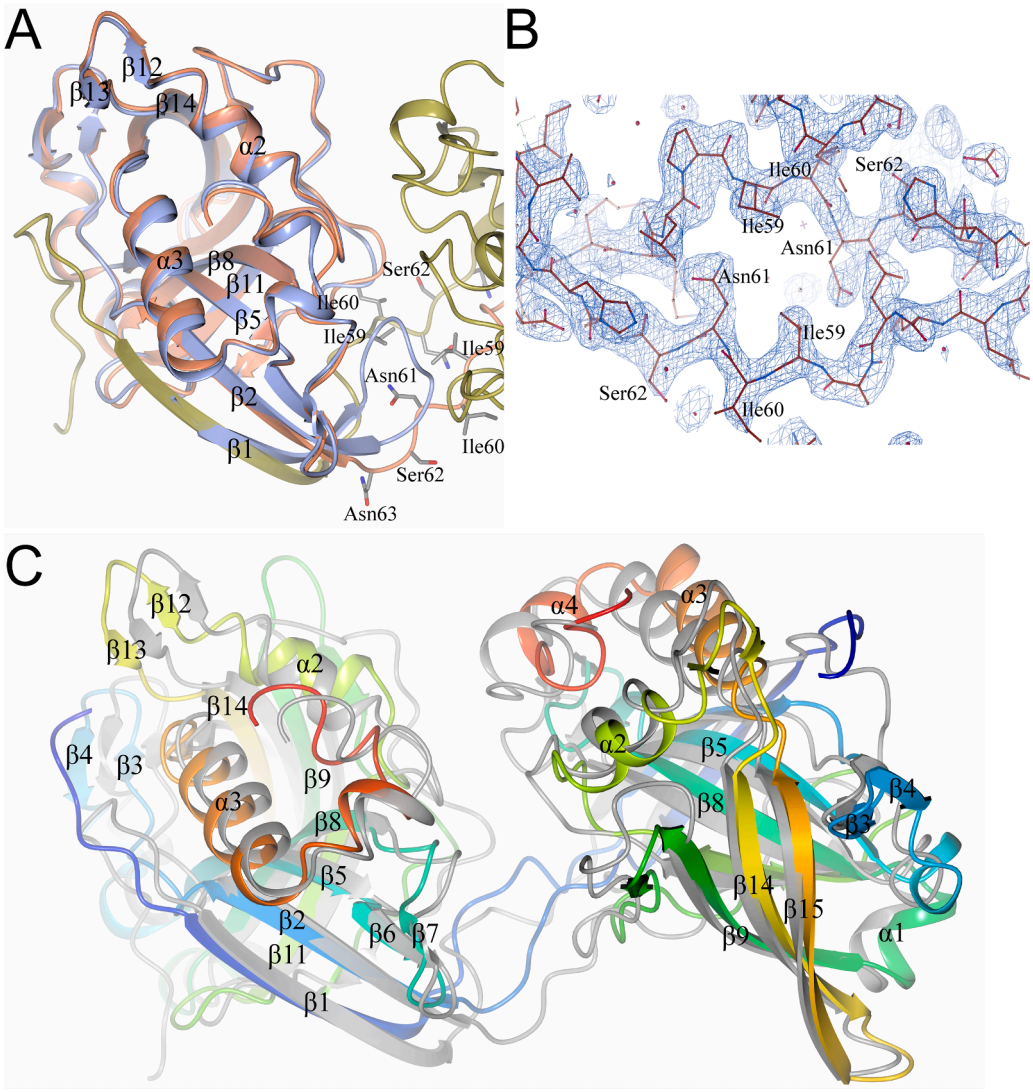

Fig. 2. Structural comparison of *B. burgdorferi* BB0158 crystal structure with the AlphaFold predicted model. (A) Superimposed AlphaFold predicted structure (blue) with the crystal structure of BB0158 where individual protomers are shown in orange and gold color accordingly (C^{α} root-mean-square deviation of 0.86). The amino acid residues within the domain-swapped dimer's loop region between β1 and β2, illustrating a major difference between the crystal structure of the homodimer and the AlphaFold-predicted monomeric BB0158, are indicated. (B) The 2Fo-Fc electron density map, contoured at 1σ, displays the loop region in the BB0158 homodimer connecting β1 and β2. This region shows a notable difference from the predicted protein model. (C) The crystal structure of BB0158 domain-swapped dimer superimposed with the AlphaFold-Multimer predicted BB0158 homodimer (C^{α} root-mean-square deviation of 2.60). The predicted structure is illustrated from blue at the N-terminus to red at the C-terminus, but the crystal structure in gray color. The four α-helices are marked from α1 to α4 and the fifteen β-strands are marked from β1 to β15.

ranked by using LDDT (pLDDT) scores).

2.5. Gel filtration chromatography

30 μL of $BB0158_{29–238}$ (2 mg/ml) in 20 mM Tris–HCl (pH 8.0) and 100 mM sodium chloride was loaded on a prepacked Superdex 200 Increase 3.2/300 column (Cytiva, MA, USA) equilibrated with the same buffer and connected to an Akta Pure 25 chromatography system (Cytiva, MA, USA). The flow rate was set to 0.05 ml/min. Ovalbumin (43 kDa) and chymotrypsinogen A (25 kDa) were used as MW reference standards.

3. Results and discussion

3.1. BB0158 forms a domain-swapped dimer

To produce the recombinant BB0158, its construct was designed to exclude the signal peptide region, specifically resides 1–20. Additionally, the AlphaFold (Jumper et al., 2021) predicted structure indicated an unstructured, low-confidence region for approximately the next 10 residues. Consequently, the construct was initiated from residue 29. The obtained crystals of $BB0158_{29–238}$ were in space group $P2_1$ with four molecules present in the asymmetric unit. The crystal structure of BB0158 was refined for residues 34–238 because the first few residues were not observed in the electron density, possibly due to the flexible nature of the N-terminal part (Fig. 1). BB0158 belongs to the α + β class of proteins and consists of eight major β-strands, along with several shorter antiparallel hydrogen-bonded regions found in loop regions between β2 and β3, as well as β3-β4. Additionally, two short α-helices are present, with one located between β6 and β7, and the other at the C-terminal end of the protein. During the molecular replacement process, we used the AlphaFold predicted model of BB0158 as the search model. This model exhibited an overall strong similarity to the crystal structure, with a C^{α} root-mean-square deviation 0.86 Å. However, there

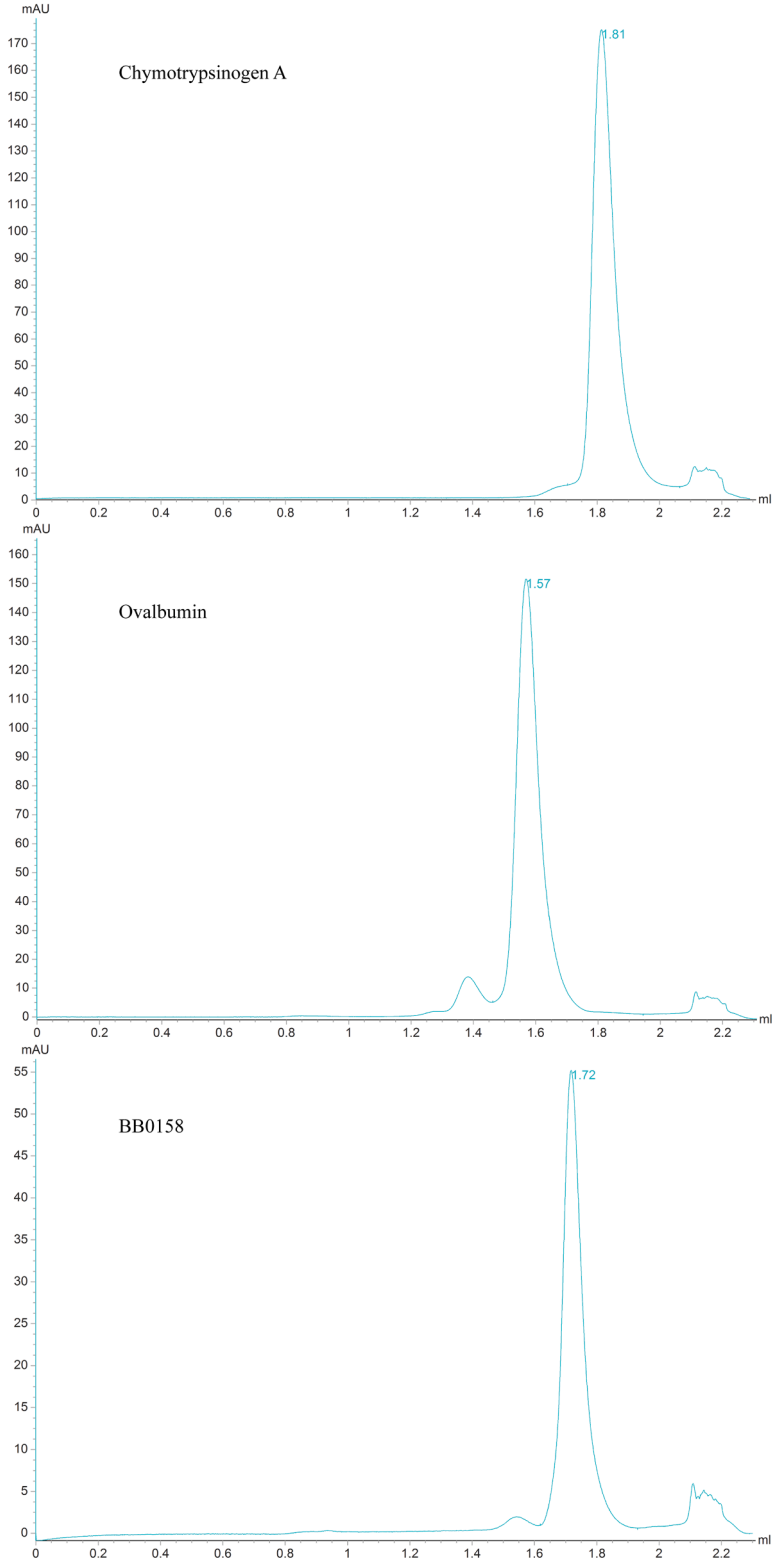

Fig. 3. The analysis of *B. burgdorferi* BB0158$_{29–238}$ (24 kDa) by size-exclusion chromatography. To estimate the molecular weight of the oligomer, calibration was performed with molecular weight reference standards, including chymotrypsinogen A (25 kDa) and ovalbumin (43 kDa).

was one major difference: the crystal structure of BB0158 revealed a domain-swapped dimer, where the β1 strand from one monomer replaced the β1 strand from the other monomer (Fig. 2A and 2B). Notably, when AlphaFold-Multimer prediction was performed for BB0158, a nearly identical result of a domain-swapped dimer was obtained (Fig. 2C). Gel-filtration chromatography of BB0158 indicated a single peak eluting between the MW standards ovalbumin (43 kDa) and chymotrypsinogen A (25 kDa), suggesting an apparent molecular weight of 32 kDa for BB0158 (Fig. 3). Theoretical MW for the monomeric form is 24 kDa while 48 kDa for the dimeric form of BB0158. Consequently, the gel filtration results are somewhat inconclusive. However, both monomers in the crystal structure produce a considerable buried surface

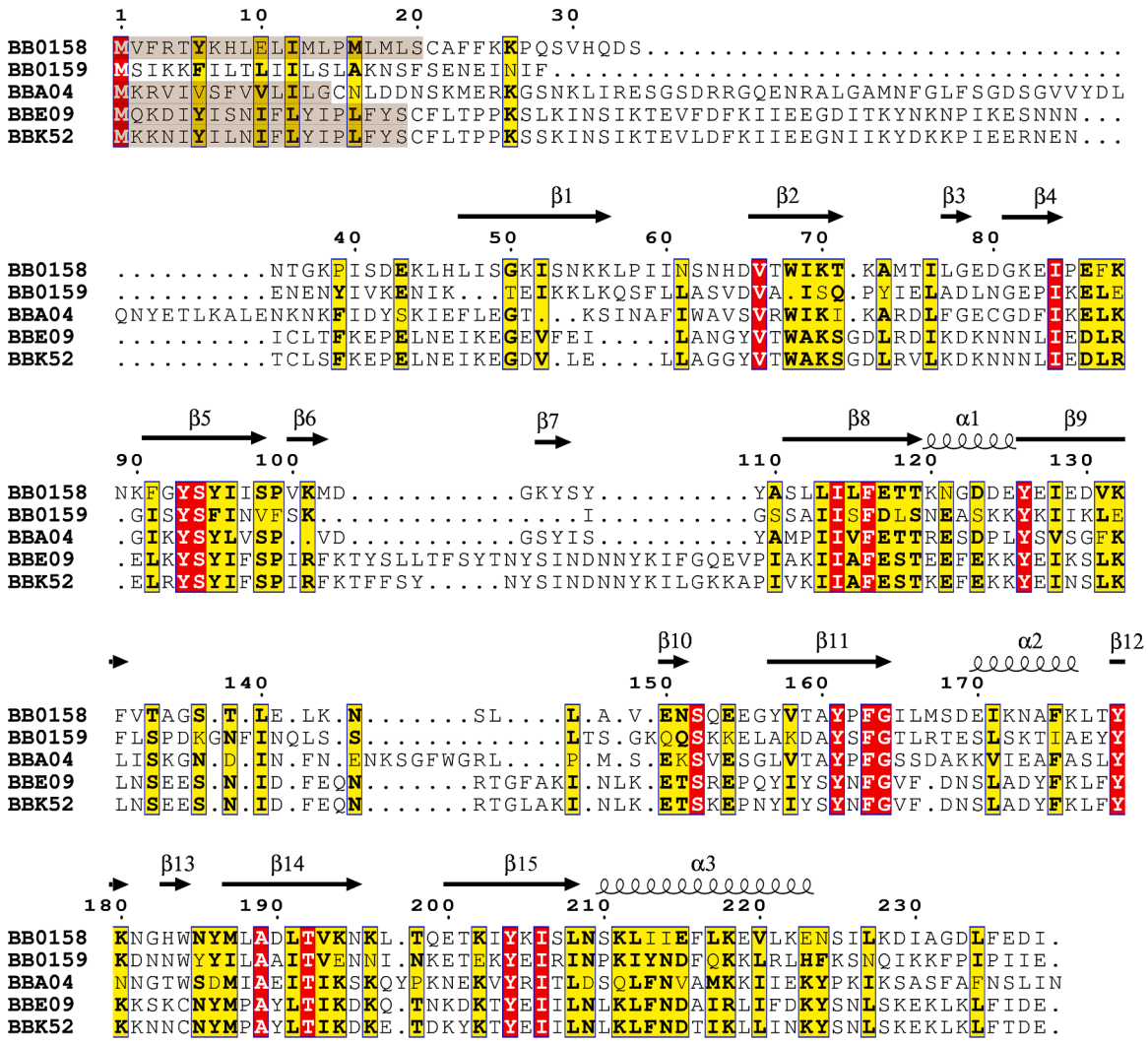

Fig. 4. Structure-based sequence alignment of the *B. burgdorferi* PFam44 members BB0158, BB0159, BBA04, BBE09 and BBK52. The sequence alignment was performed using *Clustal Omega* and then manually adjusted based on the 3D structural comparison between the crystal structure of BB0158 and the AlphaFold-predicted structures of BB0159, BBA04, BBE09, and BBK52, and processed using ESPript 3 (Robert and Gouet, 2014; Sievers et al., 2011). Fully conserved residues across these paralogous proteins are colored with a red background, while residues that are partially conserved among at least four out of the five members are marked with a yellow background. The lipoprotein signal peptide region in BB0158, BBA04, BBE09, and BBK52 has been shaded in brown. The secondary structure elements and numbering are shown for BB0158.

area of 3470 Å^2, approximately ¼ of the total accessible surface area (around 13,000 Å^2) of the individual protomers. Therefore, a compact dimer might theoretically elute later than expected.

Oligomerization through domain swapping is known as an exchange of identical structural units among protein molecules within an oligomer. This intriguing mechanism has been observed in a wide range of proteins (Bennett et al., 1994; Kundu and Jernigan, 2004; Liu and Eisenberg, 2002). The specific region that undergoes swapping between the protomers can consist of single or multiple α-helices, β-strands, or a combination of both structural elements. It is widely believed that domain swapping also serves a functional role in the biology of these proteins (Liu and Eisenberg, 2002). In cadherins, proteins essential for cell adhesion, dimerization is governed by the exchange of N-terminal β-strands (Vendome et al., 2011). This process leads to the formation of a homodimer known as a strand-swapped dimer, which plays a pivotal role in cadherins function and therefore serves as a prime target for protein inhibition (Dalle Vedove et al., 2019). Determining whether BB0158 can form a domain-swapped dimer on the cell surface of *B. burgdorferi* and revealing its specific function remain tasks for future research. Note that in *B. burgdorferi*, lipoprotein dimerization has been observed in several membrane-attached proteins, such as BBA68 (CspA), BBA73, BB0238, and OspC (Brangulis et al., 2013; Cordes et al., 2005; Foor et al., 2023; Kumaran et al., 2001). This points to a prevalent trend among lipoproteins to form dimers. However, BB0158 stands out due to its unique dimerization mechanism involving the formation of a domain-swapped dimer.

3.2. *BB0158 as a member of the PFam44*

BB0158 is part of a family of paralogous proteins found in *B. burgdorferi*, and through genome analysis, it has been classified as a member of the paralogous gene family 44 (PFam44) (Casjens et al., 2000; Fraser et al., 1997). Within the PFam44, there are five members, which include BB0158, BB0159, BBA04, BBE09, and BBK52. Furthermore, there are several regions in the *B. burgdorferi* DNA that show sequence similarity, although some of them are truncated or otherwise altered, resulting in their categorization as pseudogenes (BBE04, BBE05, BBF22, BBH36, BBQ04). BB0158 shares a sequence identity ranging from 20 % to 30 % with the other four members of the PFam44 family. Additionally, the mutual similarity between these other members is

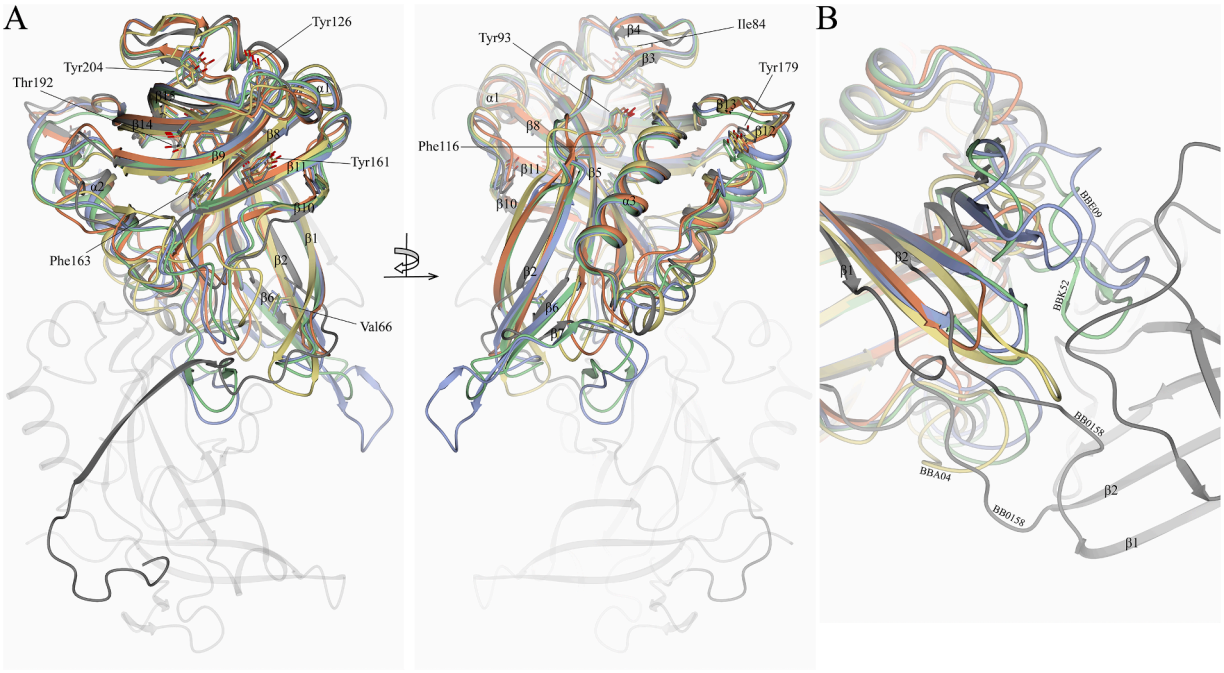

Fig. 5. (A) The crystal structure of *B. burgdorferi* BB0158 (gray) superimposed with AlphaFold predicted structure of *B. burgdorferi* BB0159 (orange), BBA04 (yellow), BBE09 (blue), and BBK52 (green). Fully conserved residues between the PFam44 members are depicted in a ball and stick representation. One of the protomers in the domain-swapped BB0158 dimer is displayed as transparent. These structures are presented from two different angles, each rotated by 180° for a comprehensive view. (B) The interface region between the domain-swapped dimer in BB0158 and the superimposed AlphaFold predicted structures of the other PFam44 members.

relatively consistent, except for BBE09 and BBK52, which exhibit a notably high mutual identity of 84 % (Fig. 4). Despite the low sequence identity, the superposition of the BB0158 crystal structure with the AlphaFold-predicted structures of the PFam44 members, including BB0159, BBA04, BBE09, and BBK52, revealed a highly conserved overall fold with a C^{α} root-mean-square deviation ranging from 1.76 to 1.96 Å (Fig. 5A). The fully conserved residues, primarily of hydrophobic nature as found from the structure-based sequence alignment, are oriented towards the interior of the proteins. These residues are thus likely important for maintaining the protein fold and are less likely to directly participate in interactions with potential ligands (Figs. 4 and 5A). While the overall structural similarity among these proteins is very high, major differences are observed in several loop regions. For instance, in BBE09 and BBK52, the region between β5 and β8 is notably extended compared to the other PFam44 members, with an additional approximately 20 residues. Similarly, the loop region between β9 and β10 is more extended in BBA04, BBE09, and BBK52 when compared to BB0158 and BB0159 (Figs. 4 and 5A). Another notable difference between the PFam44 members, evident from both sequence alignment and 3D structural analysis, is the presence of the lipoprotein signal peptide. Protein localization studies have indicated that PFam44 members BB0158, BBA04, and BBK52, are surface-exposed lipoproteins (Dowdell et al., 2017). Lipoproteins are a distinct type of proteins that possess an N-terminal signal sequence. After proteolytic cleavage of this fragment,

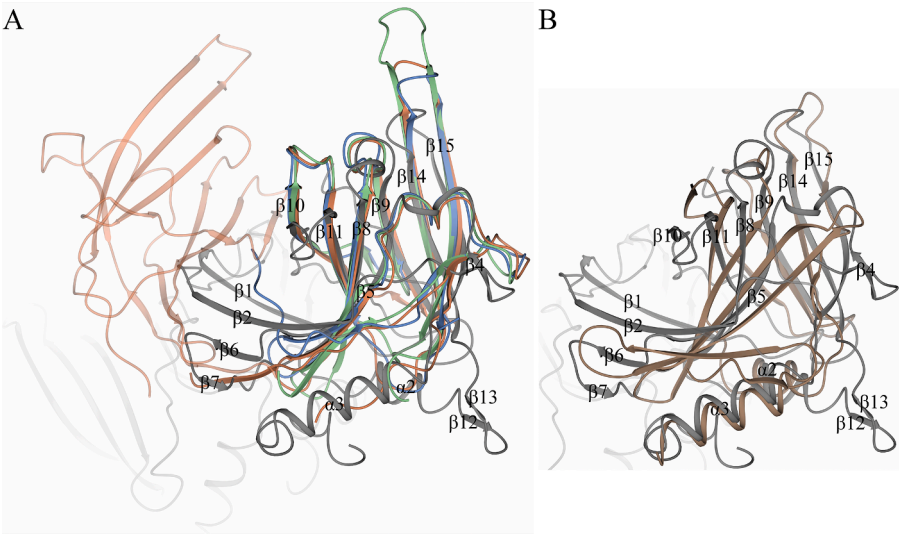

Fig. 6. (A) The *B. burgdorferi* BB0158 (gray) superimposed with the iron-regulated surface determinant (Isd) proteins IsdA (orange), IsdB (blue), and IsdC (green) from *S. aureus*. (B) BB0158 (gray) superimposed with the invasion-associated protein B from *B. henselae* (brown). The secondary structure elements are indicated for BB0158.

Table 1
PDBeFold search results against BB0158.

No.	Protein	Organism	PDB ID	Z-score	RMSD (Å)	Identity (%)	N residues
1.	Iron-regulated surface determinant protein A	*Staphylococcus aureus*	3QZP	6.3	3.3	6	125
2.	Iron-regulated surface determinant protein B	*Staphylococcus aureus*	3RUR	4.9	3.4	8	106
3.	Iron-regulated surface determinant protein C	*Staphylococcus aureus*	2O6P	5.2	3.1	7	90
4.	Invasion-associated protein B	*Bartonella henselae*	3DTD	6.2	3.3	4	118

the protein becomes covalently linked to a fatty acid moiety (Zückert, 2014). An N-terminal signal sequence, which contains a four amino acid motif known as a lipidation consensus sequence, followed by a Cys-residue where the fatty acid attaches, can be identified in BB0158, BBA04, BBE09, and BBK52 (Fig. 4). While BBE09 hasn't been studied in previous research, based on sequence analysis, the N-terminal region covering the signal peptide region indicates an 85 % identity with BBK52. Moreover, similar to BBK52, BBE09 contains all the signal peptide-specific elements defined for spirochetal lipoproteins (Fig. 4) (Setubal et al., 2006). In contrast, BB0159 lacks a Cys-residue in the unstructured N-terminal region, an essential component for covalent attachment to the cell membrane. The first 20 residues in the N-terminal region, forming a hydrophobic α-helix as indicated by the AlphaFold structure, might function as a Sec-dependent signal peptide. This presumption is further supported by SignalP 6.0 analysis (Teufel et al., 2022), indicating a probability of over 90 % for peptide processing between residues 21 and 22 by signal peptidase I. Consequently, based on the protein secretion mechanism in *B. burgdorferi* (Zückert, 2019), it is suggested that BB0159 is likely located in the periplasm as a soluble protein. The length of the unstructured N-terminal region in BB0158, BBA04, BBE09, and BBK52, which serves as a linker between the membrane and the globular domain after signal peptide processing and covalent attachment, varies among these proteins. Specifically, it consists of 16 residues in BB0158, 55 residues in both BBE09 and BBK52, but extends to 71 residues in the case of BBA04.

The domain-swapped dimer formation, as observed in the crystal structure and the AlphaFold-Multimer prediction for BB0158, was not observed for the other PFam44 members using AlphaFold-Multimer prediction. One possible explanation for the inability of BBA04 to form a domain-swapped dimer may be related to the loop regions. As mentioned earlier, the loop regions indicate the greatest variability between the PFam44 members. In BBA04, the extended loop region between β9 and β10 could potentially collide with the other loop region involved in domain-swapped dimer formation as observed in BB0158 (Fig. 5B). Similarly, in BBE09 and BBK52, the extended loop region between β5 and β8 would likely interfere with dimer formation, as evident from the superimposed structures (Fig. 5B).

3.3. BB0158 structural similarity

The analysis conducted using the PDBeFold and DALI server has revealed that BB0158 shows structural similarity with proteins that contain the near transporter (NEAT) domain, particularly those found in *Staphylococcus aureus*, as well as invasion-associated protein B from *Bartonella henselae* (Fig. 6 and Table 1). The NEAT domain proteins from *S. aureus* that show similarity to BB0158 include the iron-regulated surface determinant (Isd) proteins IsdA, IsdB, and IsdC (Fig. 6A). These proteins are components of the Isd system involved in heme uptake as a source of iron (Skaar and Schneewind, 2004). However, it's important to note that BB0158 exhibits differences in the residues within the proposed active site when compared to IsdA from *S. aureus*. Consequently, it is improbable that BB0158 can bind heme, especially given the distinct amino acid composition at the active site (Grigg et al., 2011). Furthermore, *B. burgdorferi* has adapted its proteome to function without the need for iron as a cofactor and no iron transport system has been identified in *B. burgdorferi*, further indicating that the function of BB0158 is likely unrelated to heme binding (Fraser et al., 1997; Posey and Gherardini, 2000). However, several studies have indicated that Isd proteins are multifunctional, with the ability to interact with various molecules and components such as integrins, fibrinogen, fibronectin, desquamated nasal epithelial cells, platelets, and vitronectin (Clarke et al., 2004; Corrigan et al., 2009; Miajlovic et al., 2010; Pietrocola et al., 2020; Zapotoczna et al., 2013). This suggests that BB0158, despite its differences from IsdA in heme binding, may have diverse roles and interactions within its biological context. In turn, invasion-associated protein B from *B. henselae* is believed to facilitate *B. henselae* entry into erythrocytes, emphasizing the multifunctional nature of these proteins and their potential involvement in various cellular processes beyond heme uptake (Deng et al., 2016).

4. Conclusions

This research provides valuable insights into the *B. burgdorferi* outer membrane attached lipoproteins that potentially play a role in the pathogenesis of Lyme disease. Specifically the research was focused on structural characterization of chromosomally encoded BB0158 and four of its paralogous proteins (BB0159, BBA04, BBE09 and BBK52) that together form PFam44. The characterization of BB0158 and the insights gained into PFam44 contribute significantly to the broader understanding of proteins in *B. burgdorferi*.

Accession numbers

The coordinates and the structure factors for *B. burgdorferi* BB0158 have been deposited in the Protein Data Bank with the accession number 8Q4K.

CRediT authorship contribution statement

Kalvis Brangulis: Conceptualization, Investigation, Methodology, Resources, Supervision, Validation, Writing – original draft, Writing – review & editing. **Inara Akopjana:** Investigation. **Janis Bogans:** Investigation. **Andris Kazaks:** Investigation. **Kaspars Tars:** Funding acquisition, Project administration, Writing – review & editing.

Declaration of Competing Interest

The authors declare that there is no conflict of interest in this study.

Data availability

Data will be made available on request.

Acknowledgments

This work was supported by the European Regional Development Fund grant 1.1.1.1/20/A/048. Diffraction data for *B. burgdorferi* BB0158 were collected on BL14.1 at the BESSY II electron storage ring operated by the Helmholtz-Zentrum, Berlin. We would particularly like to acknowledge the help and support of Manfred S. Weiss and Frank Lennartz during the experiment.

Supplementary materials

Supplementary material associated with this article can be found, in the online version, at doi:10.1016/j.ttbdis.2023.102287.

References

Akopjana, I., Brangulis, K., 2022. Structural analysis of the outer membrane lipoprotein BBA14 (OrfD) and the corresponding paralogous gene family 143 (PFam143) from Borrelia burgdorferi. Pathogens 11 (2), 154.

Anderson, J.F., 1989. Epizootiology of Borrelia in Ixodes tick vectors and reservoir hosts. Rev. Infect. Dis. 11 (6), S1451–S1459.

Baranton, G., Postic, D., Saint Girons, I., Boerlin, P., Piffaretti, J.C., Assous, M., Grimont, P.A., 1992. Delineation of Borrelia burgdorferi sensu stricto, Borrelia garinii sp. nov., and group VS461 associated with Lyme borreliosis. Int. J. Syst. Bacteriol. 42, 378–383.

Bennett, M.J., Choe, S., Eisenberg, D., 1994. Refined structure of dimeric diphtheria toxin at 2.0 A resolution. Protein Sci. 3, 1444–1463.

Brangulis, K., Petrovskis, I., Kazaks, A., Baumanis, V., Tars, K., 2013. Structural characterization of the Borrelia burgdorferi outer surface protein BBA73 implicates dimerization as a functional mechanism. Biochem. Biophys. Res. Commun. 434, 848–853.

Brangulis, K., Akopjana, I., Petrovskis, I., Kazaks, A., Tars, K., 2020. Structural analysis of the outer surface proteins from Borrelia burgdorferi paralogous gene family 54 that are thought to be the key players in the pathogenesis of Lyme disease. J. Struct. Biol. 210, 107490.

Brangulis, K., Jaudzems, K., Petrovskis, I., Akopjana, I., Kazaks, A., Tars, K., 2015. Structural and functional analysis of BB0689 from Borrelia burgdorferi, a member of the bacterial CAP superfamily. J. Struct. Biol. 192, 320–330.

Burgdorfer, W., Barbour, A.G., Hayes, S.F., Benach, J.L., Grunwaldt, E., Davis, J.P., 1982. Lyme disease-a tick-borne spirochetosis? Science 216, 1317–1319.

Casjens, S., Palmer, N., van Vugt, R., Huang, W.M., Stevenson, B., Rosa, P., Lathigra, R., Sutton, G., Peterson, J., Dodson, R.J., Haft, D., Hickey, E., Gwinn, M., White, O., Fraser, C.M., 2000. A bacterial genome in flux: the twelve linear and nine circular extrachromosomal DNAs in an infectious isolate of the Lyme disease spirochete Borrelia burgdorferi. Mol. Microbiol. 35, 490–516.

Casjens, S.R., Gilcrease, E.B., Vujadinovic, M., Mongodin, E.F., Luft, B.J., Schutzer, S.E., Fraser, C.M., Qiu, W.G., 2017. Plasmid diversity and phylogenetic consistency in the Lyme disease agent Borrelia burgdorferi. BMC Genomics 18, 165.

Casjens, S.R., Mongodin, E.F., Qiu, W.G., Luft, B.J., Schutzer, S.E., Gilcrease, E.B., Huang, W.M., Vujadinovic, M., Aron, J.K., Vargas, L.C., Freeman, S., Radune, D., Weidman, J.F., Dimitrov, G.I., Khouri, H.M., Sosa, J.E., Halpin, R.A., Dunn, J.J., Fraser, C.M., 2012. Genome stability of Lyme disease spirochetes: comparative genomics of Borrelia burgdorferi plasmids. PLoS ONE 7, e33280.

Clarke, S.R., Wiltshire, M.D., Foster, S.J., 2004. IsdA of Staphylococcus aureus is a broad spectrum, iron-regulated adhesin. Mol. Microbiol. 51, 1509–1519.

Cordes, F.S., Roversi, P., Kraiczy, P., Simon, M.M., Brade, V., Jahraus, O., Wallis, R., Skerka, C., Zipfel, P.F., Wallich, R., Lea, S.M., 2005. A novel fold for the factor H-binding protein BbCRASP-1 of Borrelia burgdorferi. Nat. Struct. Mol. Biol. 12, 276–277.

Corrigan, R.M., Miajlovic, H., Foster, T.J., 2009. Surface proteins that promote adherence of Staphylococcus aureus to human desquamated nasal epithelial cells. BMC Microbiol. 9, 22.

Cowtan, K., 2006. The Buccaneer software for automated model building. 1. Tracing protein chains. Acta. Crystallogr. D Biol. Crystallogr. 62, 1002–1011.

Dalle Vedove, A., Falchi, F., Donini, S., Dobric, A., Germain, S., Di Martino, G.P., Prosdocimi, T., Vettraino, C., Torretta, A., Cavalli, A., Rigot, V., Andre, F., Parisini, E., 2019. Structure-based virtual screening allows the identification of efficient modulators of E-cadherin-mediated cell-cell adhesion. Int. J. Mol. Sci. 20 (14).

Deng, H., Pang, Q., Xia, H., Le Rhun, D., Le Naour, E., Yang, C., Vayssier-Taussat, M., Zhao, B., 2016. Identification and functional analysis of invasion associated locus B (IalB) in Bartonella species. Microb. Pathog. 98, 171–177.

Dowdell, A.S., Murphy, M.D., Azodi, C., Swanson, S.K., Florens, L., Chen, S., Zückert, W. R., 2017. Comprehensive spatial analysis of the Borrelia burgdorferi lipoproteome reveals a compartmentalization bias toward the bacterial surface. J. Bacteriol. 199 (6).

Emsley, P., Cowtan, K., 2004. Coot: model-building tools for molecular graphics. Acta. Crystallogr. D Biol. Crystallogr. 60, 2126–2132.

Evans, P.R., 2011. An introduction to data reduction: space-group determination, scaling and intensity statistics. Acta. Crystallogr. D Biol. Crystallogr. 67, 282–292.

Foor, S.D., Brangulis, K., Shakya, A.K., Rana, V.S., Bista, S., Kitsou, C., Ronzetti, M., Alreja, A.B., Linden, S.B., Altieri, A.S., Baljinnyam, B., Akopjana, I., Nelson, D.C., Simeonov, A., Herzberg, O., Caimano, M.J., Pal, U., 2023. A unique borrelial protein facilitates microbial immune evasion. MBio, e0213523.

Fraser, C.M., Casjens, S., Huang, W.M., Sutton, G.G., Clayton, R., Lathigra, R., White, O., Ketchum, K.A., Dodson, R., Hickey, E.K., Gwinn, M., Dougherty, B., Tomb, J.F., Fleischmann, R.D., Richardson, D., Peterson, J., Kerlavage, A.R., Quackenbush, J., Salzberg, S., Hanson, M., van Vugt, R., Palmer, N., Adams, M.D., Gocayne, J., Weidman, J., Utterback, T., Watthey, L., McDonald, L., Artiach, P., Bowman, C., Garland, S., Fuji, C., Cotton, M.D., Horst, K., Roberts, K., Hatch, B., Smith, H.O., Venter, J.C., 1997. Genomic sequence of a Lyme disease spirochaete, Borrelia burgdorferi. NatureNature 390, 580–586.

Grigg, J.C., Mao, C.X., Murphy, M.E., 2011. Iron-coordinating tyrosine is a key determinant of NEAT domain heme transfer. J. Mol. Biol. 413 (3), 684–698.

Hu, C.M., Wilske, B., Fingerle, V., Lobet, Y., Gern, L., 2001. Transmission of Borrelia garinii OspA serotype 4 to BALB/c mice by Ixodes ricinus ticks collected in the field. J. Clin. Microbiol. 39, 1169–1171.

Iyer, R., Kalu, O., Purser, J., Norris, S., Stevenson, B., Schwartz, I., 2003. Linear and circular plasmid content in Borrelia burgdorferi clinical isolates. Infect. Immun. 71 (7), 3699–3706.

Jumper, J., Evans, R., Pritzel, A., Green, T., Figurnov, M., Ronneberger, O., Tunyasuvunakool, K., Bates, R., Zidek, A., Potapenko, A., Bridgland, A., Meyer, C., Kohl, S.A.A., Ballard, A.J., Cowie, A., Romera-Paredes, B., Nikolov, S., Jain, R., Adler, J., Back, T., Petersen, S., Reiman, D., Clancy, E., Zielinski, M., Steinegger, M., Pacholska, M., Berghammer, T., Bodenstein, S., Silver, D., Vinyals, O., Senior, A.W., Kavukcuoglu, K., Kohli, P., Hassabis, D., 2021. Highly accurate protein structure prediction with AlphaFold. Nature 596 (7873), 583–589.

Kabsch, W., 2010. Xds. Acta. Crystallogr. D Biol. Crystallogr. 66, 125–132.

Kumaran, D., Eswaramoorthy, S., Luft, B.J., Koide, S., Dunn, J.J., Lawson, C.L., Swaminathan, S., 2001. Crystal structure of outer surface protein C (OspC) from the Lyme disease spirochete, Borrelia burgdorferi. EMBO J. 20 (5), 971–978.

Kundu, S., Jernigan, R.L., 2004. Molecular mechanism of domain swapping in proteins: an analysis of slower motions. Biophys. J. 86 (6), 3846–3854.

Liu, Y., Eisenberg, D., 2002. 3D domain swapping: as domains continue to swap. Protein Sci. 11 (6), 1285–1299.

Margos, G., Wilske, B., Sing, A., Hizo-Teufel, C., Cao, W.C., Chu, C., Scholz, H., Straubinger, R.K., Fingerle, V., 2013. Borrelia bavariensis sp. nov. is widely distributed in Europe and Asia. Int. J. Syst. Evol. Microbiol. 63, 4284–4288.

McCoy, A.J., Grosse-Kunstleve, R.W., Adams, P.D., Winn, M.D., Storoni, L.C., Read, R.J., 2007. Phaser crystallographic software. J. Appl. Crystallogr. 40, 658–674.

Miajlovic, H., Zapotoczna, M., Geoghegan, J.A., Kerrigan, S.W., Speziale, P., Foster, T.J., 2010. Direct interaction of iron-regulated surface determinant IsdB of Staphylococcus aureus with the GPIIb/IIIa receptor on platelets. Microbiology (Reading) 156, 920–928.

Mueller, U., Darowski, N., Fuchs, M.R., Forster, R., Hellmig, M., Paithankar, K.S., Puhringer, S., Steffien, M., Zocher, G., Weiss, M.S., 2012. Facilities for macromolecular crystallography at the Helmholtz-Zentrum Berlin. J. Synchrotron Radiat. 19, 442–449.

Murshudov, G.N., Vagin, A.A., Dodson, E.J., 1997. Refinement of macromolecular structures by the maximum-likelihood method. Acta. Crystallogr. D Biol. Crystallogr. 53, 240–255.

Pietrocola, G., Pellegrini, A., Alfeo, M.J., Marchese, L., Foster, T.J., Speziale, P., 2020. The iron-regulated surface determinant B (IsdB) protein from Staphylococcus aureus acts as a receptor for the host protein vitronectin. J. Biol. Chem. 295 (29), 10008–10022.

Posey, J.E., Gherardini, F.C., 2000. Lack of a role for iron in the Lyme disease pathogen. Science 288 (5471), 1651–1653.

Pritt, B.S., Respicio-Kingry, L.B., Sloan, L.M., Schriefer, M.E., Replogle, A.J., Bjork, J., Liu, G., Kingry, L.C., Mead, P.S., Neitzel, D.F., Schiffman, E., Hoang Johnson, D.K., Davis, J.P., Paskewitz, S.M., Boxrud, D., Deedon, A., Lee, X., Miller, T.K., Feist, M.A., Steward, C.R., Theel, E.S., Patel, R., Irish, C.L., Petersen, J.M., 2016. Borrelia mayonii sp. nov., a member of the Borrelia burgdorferi sensu lato complex, detected in patients and ticks in the upper midwestern United States. Int. J. Syst. Evol. Microbiol. 66 (11), 4878–4880.

Radolf, J.D., Caimano, M.J., Stevenson, B., Hu, L.T., 2012. Of ticks, mice and men: understanding the dual-host lifestyle of Lyme disease spirochaetes. Nat. Rev. Microbiol. 10 (2), 87–99.

Robert, X., Gouet, P., 2014. Deciphering key features in protein structures with the new ENDscript server. Nucleic. Acids. Res. 42, W320–W324.

Rudenko, N., Golovchenko, M., Grubhoffer, L., Oliver Jr., J.H., 2011. Updates on Borrelia burgdorferi sensu lato complex with respect to public health. Ticks Tick Borne Dis 2 (3), 123–128.

Setubal, J.C., Reis, M., Matsunaga, J., Haake, D.A., 2006. Lipoprotein computational prediction in spirochaetal genomes. Microbiology (Reading) 152, 113–121.

Sievers, F., Wilm, A., Dineen, D., Gibson, T.J., Karplus, K., Li, W., Lopez, R., McWilliam, H., Remmert, M., Soding, J., Thompson, J.D., Higgins, D.G., 2011. Fast, scalable generation of high-quality protein multiple sequence alignments using Clustal Omega. Mol. Syst. Biol. 7, 539.

Skaar, E.P., Schneewind, O., 2004. Iron-regulated surface determinants (Isd) of Staphylococcus aureus: stealing iron from heme. Microbes Infect. 6 (4), 390–397.

Stanek, G., Reiter, M., 2011. The expanding Lyme Borrelia complex–clinical significance of genomic species? Clin. Microbiol. Infect. 17 (4), 487–493.

Teufel, F., Almagro Armenteros, J.J., Johansen, A.R., Gislason, M.H., Pihl, S.I., Tsirigos, K.D., Winther, O., Brunak, S., von Heijne, G., Nielsen, H., 2022. SignalP 6.0 predicts all five types of signal peptides using protein language models. Nat. Biotechnol. 40 (7), 1023–1025.

Vendome, J., Posy, S., Jin, X., Bahna, F., Ahlsen, G., Shapiro, L., Honig, B., 2011. Molecular design principles underlying beta-strand swapping in the adhesive dimerization of cadherins. Nat. Struct. Mol. Biol. 18 (6), 693–700.

Winn, M.D., Ballard, C.C., Cowtan, K.D., Dodson, E.J., Emsley, P., Evans, P.R., Keegan, R. M., Krissinel, E.B., Leslie, A.G., McCoy, A., McNicholas, S.J., Murshudov, G.N., Pannu, N.S., Potterton, E.A., Powell, H.R., Read, R.J., Vagin, A., Wilson, K.S., 2011. Overview of the CCP4 suite and current developments. Acta. Crystallogr. D Biol. Crystallogr. 67, 235–242.

Zapotoczna, M., Jevnikar, Z., Miajlovic, H., Kos, J., Foster, T.J., 2013. Iron-regulated surface determinant B (IsdB) promotes Staphylococcus aureus adherence to and internalization by non-phagocytic human cells. Cell. Microbiol. 15 (6), 1026–1041.

Zückert, W.R., 2014. Secretion of bacterial lipoproteins: through the cytoplasmic membrane, the periplasm and beyond. Biochim. Biophys. Acta 1843 (8), 1509–1516.

Zückert, W.R., 2019. Protein secretion in spirochetes. Microbiol. Spectr. 7 (3) https://doi.org/10.1128/microbiolspec.PSIB-0026-2019.